Int. J. Heat Mass Transfer. Vol. 34, No. 4/5, pp. 949-960, 1991
Printed in Great Britain

0017-9310/91 $3.00+0.00

Measurement of local convective heat transfer coefficients using three-dimensional interferometry

S. BAHL† and J. A. LIBURDY
Thermal Fluid Laboratory, Department of Mechanical Engineering, Clemson University, Clemson, SC 29634, U.S.A.

(*Received* 31 *January* 1990 *and in final form* 5 *June* 1990)

Abstract—The reconstruction of the three-dimensional temperature distribution above a horizontal heated disk in air is used to determine the local heat transfer coefficients. Holographic interferometry is used to obtain instantaneous, three-dimensional information on the local index of refraction distribution. Several reconstruction procedures are tested under the constraints of limited field of view and limited fringe order data. These techniques are used to accurately measure the instantaneous local temperature distribution. Subsequently, the surface temperature gradients are specified by curve fitting procedures and the local heat transfer coefficients determined. The surface averaged Nusselt number agrees very well with previous studies in the literature. Real time holographic interferometry is also used to suggest some of the dynamic characteristics of the convective heat transfer process. Results show local instabilities in the form of distributed bursting of thermal energy from the surface. Also, at sufficiently high surface temperatures the entire temperature field shows evidence of oscillation or pulsation which indicates a global heat release mechanism.

INTRODUCTION

THE ABILITY to determine the local three-dimensional temperature distribution and/or local heat transfer coefficients at a surface is very important in many applications. In particular, it is often necessary to obtain such information in situations that are very sensitive to the evasive tendencies of probes. Natural convection situations are one such example where the local temperature distribution and the resultant heat transfer rate may be significantly altered by the presence of thermocouples or other probes. Moreover, it may be of concern to obtain information of the three-dimensional characteristics of the heat transfer process in a dynamic situation. This would require a large number of probes simultaneously recording the local data. It is the purpose of this paper to demonstrate the capability of obtaining instantaneous three-dimensional local temperature distributions and resultant local heat transfer rates. The techniques are equally applicable to natural and forced convection, and can also be extended to other applications such as certain fluid flow analyses.

In this study, natural convection above a horizontal heated disk was investigated using holographic interferometry. Both real time and dual exposure techniques were used. The real time method was used to qualitatively investigate the dynamic characteristics of the thermal structure. The dual exposure method was used to obtain quantitative data to evaluate the thermal field above the disk. The results are compared to data obtained with a very fine wire resistance probe as well as numerical solutions of the temperature field assuming a laminar thin layer approximation to the region near the disk surface.

Natural convection from different horizontal surfaces has been studied experimentally by Husar and Sparrow [1], Rotem and Claassen [2], Pera and Gebhart [3] and others. Analytical studies are reported by Stewartson [4], Ackroyd [5], Robinson and Liburdy [6] and others. Numerical investigations are reported by Goldstein and Lau [7], Tsai and Liburdy [8], and others. There is not very good agreement, however, on the overall (mean) heat transfer coefficient. The relatively broad range of correlations is documented by Goldstein and Lau [7]. Some general observations can be made concerning the process. The convective flow is generally agreed to being with a thin-layer flow inward along the surface. The flow eventually separates caused either by local instability or by the mixing of the induced flow from the surrounding sides of the heated surface. The local heat transfer coefficients tend to be large near the edge of the surface and approach a minimum near the center. There is some evidence of local minima away from the center reported by Al-Arabi and El-Riedy [9]. Also, at relatively high surface temperature there can be large amplitude, generally low frequency, temperature oscillations in the region above the surface. The changing nature of the fluctuations in the vicinity of the surface is described in ref. [10]. Two-dimensional interferograms used by Yousef *et al.* [11] document the large variations (−35 to 45%) of the spatially averaged Nusselt number.

The techniques used in this study to evaluate the

† Present address: Systron Donner Corp., Concord, CA 94518, U.S.A.

NOMENCLATURE

a	disk radius
d	disk diameter
E	error criteria
f	function to be reconstructed
g	gravitational acceleration
Gr	Grashof number based on L, $g\beta L^3(T_s-T_a)/\nu^2$
Gr_a	Grashof number based on length scale a
k	thermal conductivity
L	length scale, disk surface divided by the disk perimeter
Nu	mean Nusselt number based on L, hL/k
P	projection data set
Pr	Prandtl number, ν/α
r	radial coordinate (zero at disk center)
Ra	Rayleigh number, $Gr\ Pr$
T	temperature
T_a	ambient temperature
T_s	disk surface temperature
x	horizontal coordinate (zero at disk center)
y	horizontal coordinate (zero at disk center)
z	vertical coordinate (zero at disk center).

Greek symbols

α	thermal diffusivity
β	thermal expansion coefficient
η	non-dimensional variable, $Gr_a^{1/5}(z/a)[(a-r)/a]^{-2/5}$
θ	transformed coordinate, non-dimensional temperature, $(T-T_a)/(T_s-T_a)$
ν	dynamic viscosity
ρ	transformed coordinate
ϕ	viewing direction, arbitrary reference.

three-dimensional characteristics of the convection process have been modified to account for some of the unique and restrictive conditions associated with obtaining local heat transfer data. Reconstruction of the temperature field is accomplished by obtaining three-dimensional refractive index distributions from multidirectional interferometric data. For the situation of a heated disk in a large environment, the extent of the domain of interest is ill-defined. This requires the use of an envelope function to specify the reconstruction. Further, in most experimental arrangements the field of view is restricted to be significantly less than the desired 180° required for a complete data set. There are a number of reconstruction methods that have been developed which can overcome these conditions to varying degrees of accuracy. Most of these methods can be classified as either transform or series expansion methods. We have performed a detailed analysis of four of these methods. An evaluation of the results is presented in ref. [12]. Here we present the results of reasonably accurate reconstructions of thermal fields. It should be kept in mind that a great amount of work is still required to develop more generalized and rapid reconstruction procedures. A few previous studies have been presented in the literature which attempt three-dimensional reconstruction of temperature fields, namely Sweeney and Vest [13] and Vest and Radulovic [14].

EXPERIMENTAL APPARATUS AND PROCEDURE

The test apparatus was designed to measure the heat transfer rate from an isolated heat source. The geometry is a heated horizontal copper disk in air surrounded by an extended horizontal surface at ambient temperature. A cooling jacket was used to eliminate indirect heating of the extended surface caused by radial heat loss from the assembly below the surface. A schematic of the apparatus is shown in Fig. 1. The surface temperature was measured to be isothermal to within 0.5°C using thermocouples at three locations 0.5 mm below the surface. The extended surface was constructed of 0.4 mm thick balsa wood with a thin knife edge formed at the interface with the heated disk. Based on one-dimensional analysis, the extended surface temperature was calculated to decay to the ambient temperature within 3 mm of the heated disk edge for the maximum disk temperature used in the experiments. This was verified by placing a thermocouple on the surface and recording its temperature during preliminary tests. Further details of the apparatus are given in ref. [10].

The apparatus was placed on a vibration isolation table housed in an environmentally controlled room. Also, the entire tabletop was enclosed to prevent drafts. A venting system was used at the top of the enclosure to assure no stratification during the experiments. The ambient temperature was measured at three elevations during each experimental run. The temperatures always remained constant to within 1°C. Also on the table were the optical components of a holographic interferometer. The optical set-up is shown in Fig. 2. Two separate holograms were formed simultaneously for each data set. One, indicated as HP1 in the figure, was a result of diffuse illumination provided by two object beams transmitted through a set of diffusers which formed approximately a 60° field of view around the apparatus. The second hologram was formed with a collimated beam producing a two-dimensional hologram at HP2. This second hologram was used to extend the field of view. This was necessary, based on the reconstruction of com-

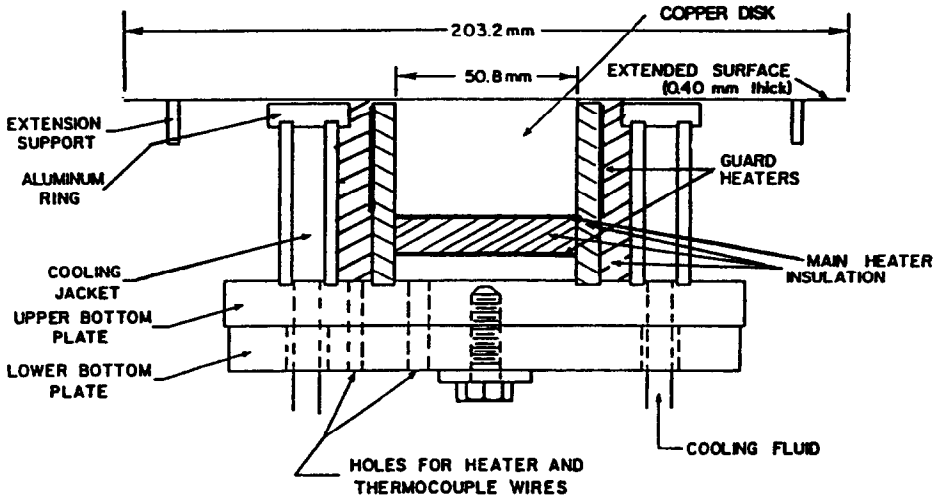

FIG. 1. Schematic of the test apparatus.

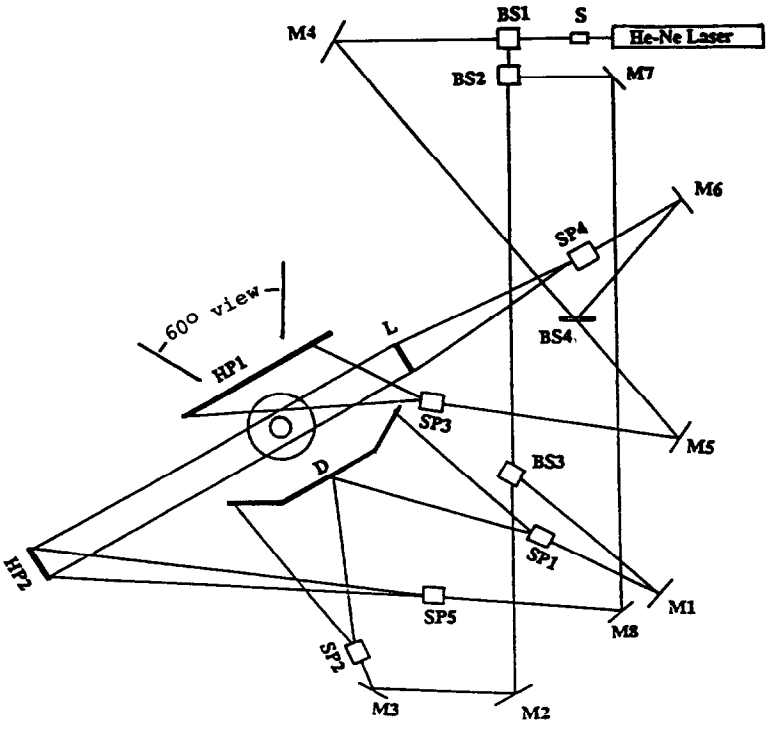

SP - Spatial Filter BS - Beam Splitter D - Diffuser
HP - Holographic Plate M - Mirror
L - Collimating Lens S - Shutter

FIG. 2. Schematic of the optical setup.

puter generated data, in order to accurately reconstruct highly asymmetric temperature distributions as determined in ref. [12]. Exposure times were approximately 0.5 s with a 15 mW helium–neon laser. Data presented here are for surface temperatures of 120 and 191°C with ambient temperatures of 25°C, which correspond to Grashof numbers of 1.36×10^4 and 1.56×10^4, respectively (using a length scale of the disk surface area per disk perimeter, and properties evaluated at the arithmetic mean of the disk surface and ambient temperature).

The data acquisition consisted of a series of photographs of each reconstructed hologram at discrete viewing directions over the field of view. A total of 15 viewing directions over the 60° field of view were used for the lower surface temperature; a total of 13 views were used for the higher temperature. In addition, a single view was added representing the data on HP2 which was at 90° to the central viewing direction of HP1. The holograms were formed at least 15 min after the disk surface temperature reached a steady uniform temperature. The data were in the form of photographs of the fringe locations from the reconstructed holograms at each viewing direction. An example is shown in Fig. 3. The coordinate represents the position along a line normal to the viewing direction, ρ. There is uncertainty associated with camera alignment, location of the fringe position in each photograph relative to an absolute reference (disk coordinates), and identification of the appropriate fringe location (fringe width). To reduce some of these errors a series of fiducial pins were placed around the disk for alignment through the camera lens system which was operated with a small aperture. The fringe order data were extracted from the photographs by projecting the negatives onto a large screen. The screen had a grid superimposed on it which was scaled for the particular view being analyzed. The geometric center of a fringe, when scanned horizontally, was chosen as the fringe order location. An estimate of the errors associated with the identification of the fringe location was made by varying the location input into the reconstruction procedures and noting the effects on the predicted temperature fields. Fringe location and other uncertainties associated with the reconstruction procedure were taken into consideration and are discussed later.

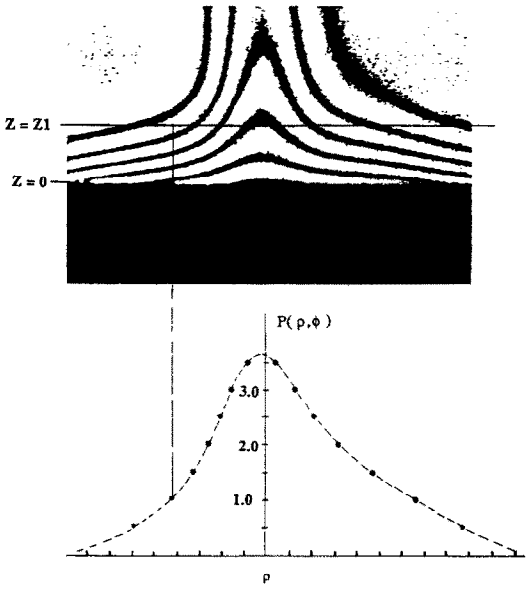

FIG. 3. Sample data set from one view and the distribution of fringe order data.

RECONSTRUCTION PROCEDURE

The three-dimensional reconstruction was accomplished by independently examining a series of horizontal planes above the disk. The problem then becomes one of a two-dimensional reconstruction of the function $f(x, y)$ from projection data (fringe order data), $P(\rho, \theta)$, shown in Fig. 3. The projection data represents the line integral information of the light paths through the index of refraction field to be evaluated. This is equivalent to the Radon transform of the index of refraction distribution, as described by Vest [15], and can be written as

$$\Delta\Phi(\rho, \theta) = \int [n(x, y) - n_0]\, ds = P(\rho, \phi)\lambda$$

$$= \iint [n(x, y) - n_0]\delta(x\cos\phi + y\sin\phi - \delta)\, dx\, dy \quad (1)$$

where $\Delta\Phi$ is the light path length difference caused by the variation of the index of refraction from the ambient value, $(n(x, y) - n_0)$, λ the wavelength of the light source and δ the Dirac delta function. The integration in equation (1) is taken along the path defined by ρ and ϕ through the field of interest. The local distribution of the index of refraction relative to the ambient represents the function $f(x, y)$ to be evaluated.

The reconstruction process is one of inverting equation (1) to obtain the spatial variation of the index of refraction over the region of interest. The unspecified extent of the integration introduces further complexities, especially in the present situation where the thermal field asymptotically approaches the ambient condition. This is handled by introducing an envelope function, as previously mentioned, which describes the variation of the index of refraction in the outer edges of the region of interest. This is included in a later section which discusses uncertainty.

Many methods exist for the reconstruction of phase objects. Most methods can be classified as either transform or series expansion methods. All such methods provide greatest accuracy when a full 180° field of view is available. In this study, four different methods were evaluated, two transform methods (filtered-backprojection and the direct Fourier transform) and

two series expansion methods (sine expansion and an iterative method). Each of these methods was assessed for the accuracy of reconstruction using computer generated data sets of complex index of refraction distributions. These distributions were chosen so as to evaluate the reconstruction of high spatial frequency content and the effects of limited field of view. A description of the error analysis as it pertains to the present problem is provided in a later section of this paper. A detailed discussion of the four methods and the associated reconstruction errors are provided in refs. [12, 16]. In this paper we present results using the iterative series expansion method since its reconstruction errors are at or below the errors associated with the other methods.

The series expansion method obtains a reconstructed function based on the following representation:

$$f(x, y) = \sum_{i=1}^{L} c_i b_i(x, y) \tag{2}$$

where $b_i(x, y)$ represents a basis function, c_i is a real coefficient and the series expansion is in L terms. Due to the linearity of the Radon transform the series representation can be operated on to relate experimental data to the unknown coefficients, c_i. Several different types of basis functions have been used, such as those used by Cormack [17], Bracewell and Wernecke [18], Cha [19] and others.

The iterative method used here is a form of the algebraic reconstruction technique (ART). This method describes the projection data as a series of discrete weighted functions within a grid which extends over the region of interest. A light ray is defined to be of finite width passing through the phase object at a specific viewing angle. Each grid subregion has an assumed distribution of the index of refraction. The reconstructed function values are iterated constrained by the given projection values over a series of viewing directions. The iteration proceeds until a specified convergence criteria is met, such as a maximum value of the global error associated with the projection of the reconstructed function and the actual projection data. General information on the technique is given by Oppenheim [20] and a description of ART is given by Gordon [21].

In the evaluation of the performance of the reconstruction the following factors were considered: (i) the ability to resolve high spatial frequency information, (ii) the effect of limited field of view and a limited number of viewing angles, and (iii) the uncertainty caused by noisy data. The performance of each method was determined based on different sampling grids coupled with different fields of view. Reconstruction errors associated with (i) and (ii) generally decrease with increasing field of view and are highly dependent on the function being evaluated. As an indication of the magnitude of the errors associated with the reconstruction, computer generated data sets were used which were in the form of two-dimensional asymmetric Gaussian and double peaked Gaussian functions. The normalized residuals at all the sample points for a 45° field of view were 2.0–7.0% provided a normal viewing direction, equivalent to hologram HP2 defined previously, was used. The percent errors of the peak values were 0.3–7.6%. Further details of the errors associated with items (i) and (ii) listed above are presented in refs. [12, 16].

UNCERTAINTY OF THE EXPERIMENTAL RESULTS

In this experimental method, errors are introduced by noise inherent in the reconstruction procedure and in data acquisition. Each of these were studied and are presented below. Reconstruction errors associated with uncertainty of the fringe order data are evaluated first. Then, errors associated with the acquisition of data in the experimental setup are evaluated.

Effect of noise in reconstruction

The effect of noise in the fringe data on the reconstructed temperature was determined by carrying out a series of computational experiments using computer generated data. The study was carried out by first creating data sets consisting of discrete projection values and their associated spatial locations. Gaussian noise was added to the spatial locations to simulate the uncertainty in the fringe location. The projection values were obtained corresponding to the perturbed spatial location data and assigned to the original set of spatial locations. The resulting noise associated with the projection data, P', is characterized by the normalized residual $C1 = \|P - P'\|/\|P\|$ where P represents the actual projection value and P' the value associated with the noisy data at the same corresponding location. The effect of noise was evaluated using the normalized residual based on subsequent iteration function values, $C2$, and the normalized residuals based on the actual and the reconstructed function values, $C3$. The errors associated with the fringe noise were determined after each iteration of the reconstruction procedure.

For a double Gaussian function with a 90° field of view, and a noise level $C1$ between 0.5 and 9.0% the residual $C2$ is below 2%. For all values of noise, $C2$ is a monotonically decreasing function of iteration number, a typical value after 30 iterations being 0.5%. Unlike the behavior of $C2$, $C3$ reaches a minimum when evaluated vs the number of iterations. This trend is shown in Fig. 4 for four different noise levels. The minima of $C3$ occur at the iteration when the value of $C2$ is nearly that of the noise level. As the number of iterations increases the residual $C2$ decreases below the noise level $C1$, and the residual $C3$ increases. Also, in the situation of large noise levels the number of iterations required to reach the minimum in the residual $C2$ decreases and the slope of the curve preceding the minimum increases. For example, the

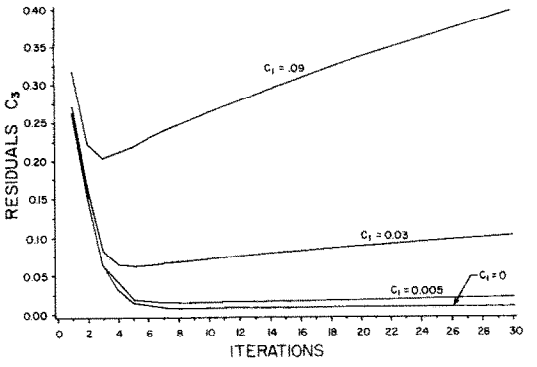

FIG. 4. Residual $C3$ vs number of iterations for various levels of noise, $C1$, using the iterative method with a 90° field of view.

number of iterations required to obtain a minimum residual when $C1$ is 0.5 and 9.0% is 8 and 3, respectively. It is concluded, that in the presence of noise the reconstruction process should be stopped after an optimum number of iterations in order to obtain the best results. This optimum value is dependent on the estimation of the noise in the fringe order data.

Another concern is the convergence of the iteration scheme in the presence of noise. When low noise levels were used with the computer generated data the function values were found to converge within a few iterations. However, at high noise levels the reconstructed values did not converge and in some cases oscillation of the predictions increased with the number of iterations.

Temperature evaluation from experimental data

In addition to the uncertainties associated with reconstruction from the fringe order data sets, there are also uncertainties associated with the evaluation of the temperature in the region of interest from the experimental data. The data sets consisted of the projection data for the two surface temperatures. The temperatures were reconstructed at elevations of 1, 2 and 3 mm using a uniform 21×21 grid centered above the disk. Five different reconstruction regions were used. The extent of the regions varied from $1.68d$ to $2.52d$ beyond the edge of the disk (where d is the disk diameter). It was found that there is a small effect of the extent of the domain on the reconstructed temperature field. Between the two extremes of $1.68d$ and $2.52d$ the temperature above the center of the disk varied by 1.5 to 3% depending on the surface temperature and the elevation. Based on these results a compromise between grid resolution and domain size resulted in a 21×21 grid with an extent of $2.1d$.

As is shown in Fig. 3, the data is discrete to within a fringe order number of 0.5. The exact location of the zero fringe order cannot be determined. The location of the zero-order fringe was determined by applying a Gaussian envelope function to the tails of the projection distribution (fringe order number). A Gaussian function was chosen because it is thought to closely approximate the actual temperature decay. Some of the consequences associated with truncation errors are discussed by Bracewell and Wernecke [18] and Cha [19] for a limited field of view. In addition, the fringe order data were interpolated using a cubic spline to obtain a higher density of data. The spline fit and the Gaussian tails were forced to match smoothly at a fringe order number of 0.5. Variations applied to the specific Gaussian function showed very little effect on the reconstructed temperatures except in the extreme outer regions.

Experiments were carried out to estimate the magnitude of the noise in the fringe order data and thus obtain an optimal number of iterations to be used in the reconstruction of the temperatures. Two error criteria were used, $E1$ and $E2$. $E1$ is a measure of the noise in the projection data caused by the inexact ability to locate the fringe data and is defined in a manner similar to $C1$. The magnitude of $E1$ was estimated by adding Gaussian noise to the experimental data with a standard deviation of up to 15% of the local fringe spacing. For a noise level equivalent to a 5% standard deviation, the value of $E1$ is approximately 1% and rises to near 3% for a standard deviation of 15%. $E2$, a slightly modified version of $C2$, is the norm of the reconstructed temperature based on the previous iteration, that is

$$E2 = \frac{\| T^i - T^{i-1} \|}{\| T^i \|} \tag{3}$$

where T^i and T^{i-1} are the temperatures after the i and $i-1$ iterations, respectively. This definition, which is based on T^i, is necessary because the true temperature value is not known. However, for a converging solution this should provide a good estimate of $C2$. For all data sets, the value of $E2$ decayed to approximately 1% after five iterations and less than 0.5% after ten iterations. Based on the numerical experiments mentioned in the previous section the relative magnitudes of $E1$ and $E2$ were used to select the number of iterations to obtain the best estimation of the temperature distribution. The choice of the number of iterations is also influenced by the variation of the local temperature over the domain of reconstruction. Following the foregoing procedure the optimum number of iterations used for the reconstruction of the temperatures was found to be four. For further details see ref. [16].

Since it is the index of refraction that is being reconstructed the associated error in the predicted temperature depends on the temperature–index of refraction relationship. Using the Gladstone–Dale relationship [15] and a perfect gas relationship there is a 0.94% error of temperature for a 1% error of index of refraction at 100°C and a 1.27% error at 170°C. For the temperatures calculated here the relationship between the index of refraction and temperature for air given by Radulovic [22] was used, this is claimed to be more accurate.

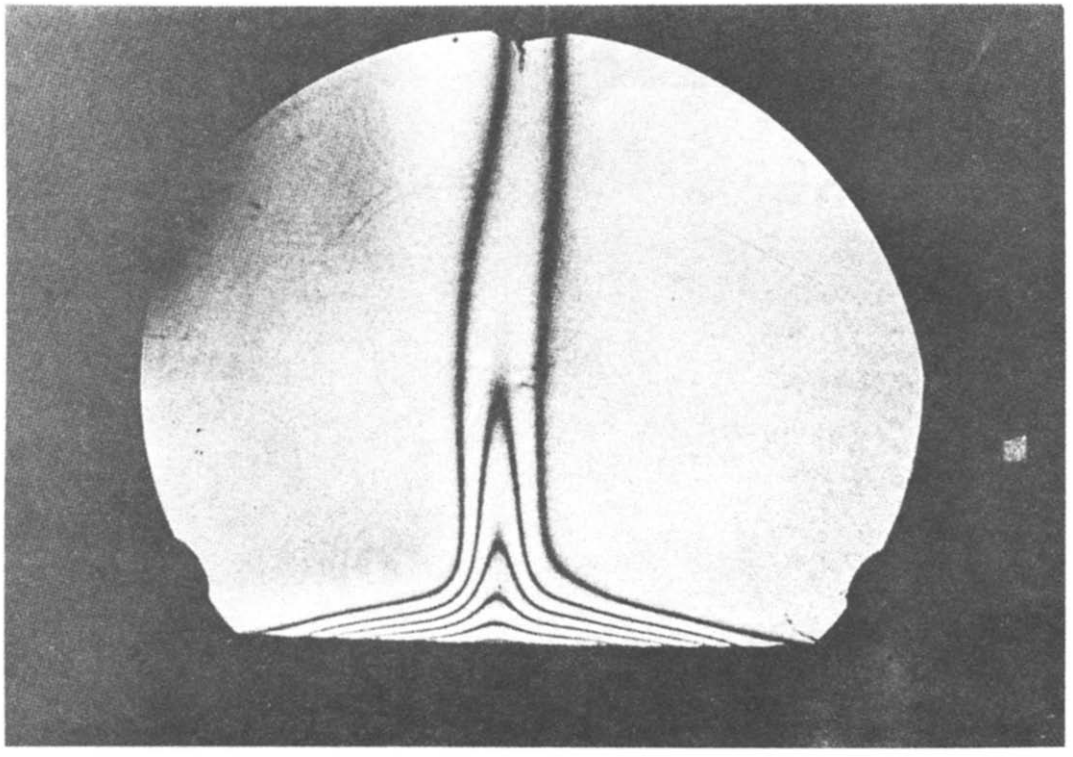

(a)

(b)

FIG. 5 (*continued overleaf*).

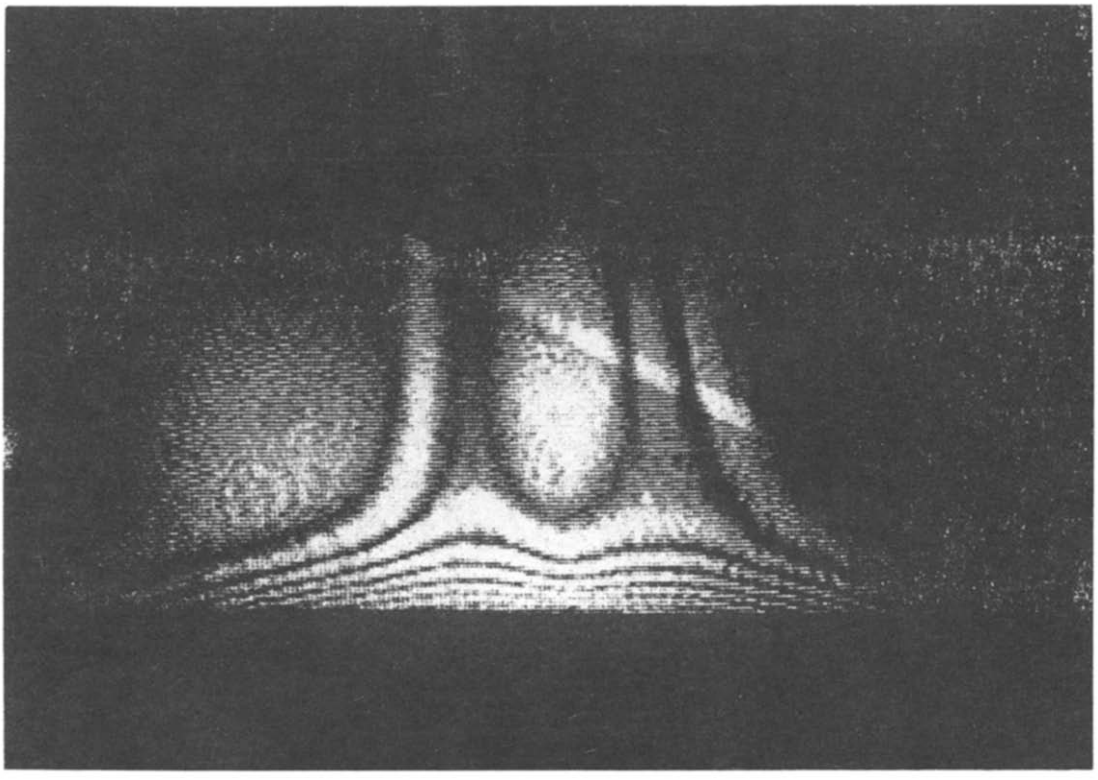

(c)

FIG. 5. Real time interferograms: (a) $T_s = 130$ C, (b) $T_s = 177$ C, (c) $T_s = 158$ C with T_a approximately 25 C in each case.

Lastly, some error is introduced in the evaluation of the temperature gradients at the wall. Four different polynomial curve fitting schemes were used. These were based on the surface temperature and on the reconstructed temperatures at discrete locations above the disk. A cubic polynomial was chosen based on the observation that it provided the smoothest fit of the data. An alternative method, which was not used here, is to surface fit the data at each elevation and then evaluate the surface gradients where desired.

RESULTS

The results are presented in two parts, the qualitative evaluation of the real time interferograms and the quantitative results of the reconstructed temperatures. Results are compared with both numerical predictions and fine wire probe measurements made above the same apparatus. Also, the surface averaged instantaneous heat transfer coefficient results are compared to correlations in the literature.

The real time interferograms presented here are two-dimensional representations of the three-dimensional events. However, they provide meaningful indicators of the nature of the convection process. At very low surface temperatures a thin layer develops inward from the leading edge. As the surface temperature is increased a narrow plume develops at the center of the disk. At low temperatures the plume is steady, only slight inconsequential swaying is observed. Figure 5(a) indicates the structure of such a plume where the disk surface temperature is 130°C and the ambient temperature is 25°C. As the surface temperature is increased, the plume begins to sway more rapidly. At still higher surface temperatures, the entire structure begins to display dynamic character. The fringes near the surface rise and fall in unison, there is a wave like motion across the disk, the fringes near the center and sometimes near the edge of the disk periodically rise and burst open indicating a rising packet of hot fluid. This bursting phenomena is depicted in Fig. 5(b), for a surface temperature of 177°C and an ambient temperature of 24.5°C. Intermittent with this sporadic bursting the entire fringe pattern oscillates up and down in unison at about 0.5–1.0 Hz. At somewhat lower surface temperatures a structure like that shown in Fig. 5(c) appears. This pattern sometimes alternates with a fringe pattern similar to that shown in Fig. 5(b). It is apparent that the three-dimensional structure is based on a complex flow and thermal distribution that is sensitive to the surface temperature.

The temperatures were reconstructed at elevations of 1, 2, and 3 mm above the surface for the two surface temperatures given previously. Figures 6 and 7 illustrate the temperature distributions. The fairly uniform distribution at the lower elevation evolves to the more plume-like Gaussian distribution at higher elevations. Comparison is made between the reconstructed temperatures and those measured with a fine wire resistance probe [10], in Fig. 8 in the region above

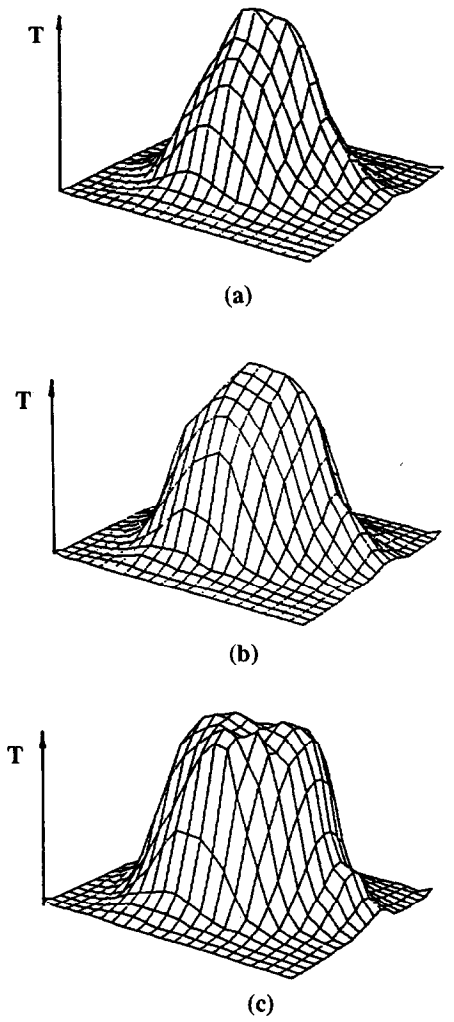

FIG. 6. Reconstructed temperatures for a surface temperature of 120°C at elevations of (a) 3 mm, (b) 2 mm, and (c) 1 mm.

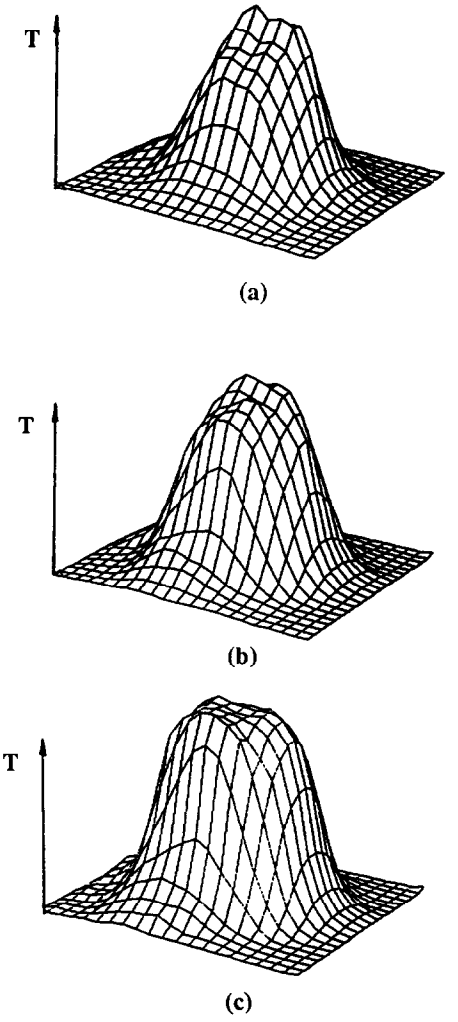

FIG. 7. Reconstructed temperatures for a surface temperature of 191°C at elevations of (a) 3 mm, (b) 2 mm, and (c) 1 mm.

the disk centerline. It should be noted that there were significant temporal temperature fluctuations measured by the probe. The vertical bars shown in the figure represent the extent of the three standard deviation limits during the fluctuations in the temperature–time traces of the probe measurements. Details of the spectral character of these data are given in ref. [10]. Although not shown, the reconstructed temperatures were compared with the probe data at four circumferential positions for several radial locations for the two surface temperature conditions. In general, the reconstructed temperatures are well within the three standard deviation limits of the probe data except for two points very near the surface.

Numerical results from ref. [8] are compared to the reconstructed temperatures in Fig. 9. The numerical results assume laminar, axially symmetric flow and

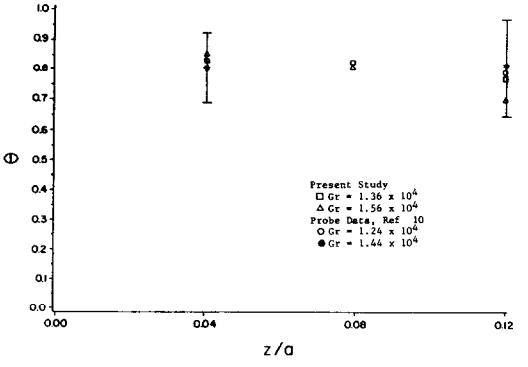

FIG. 8. Comparison of reconstructed temperatures with probe measurements above the center of the disk; bars represent three standard deviation limits of fluctuating temperature measurements made with the probe.

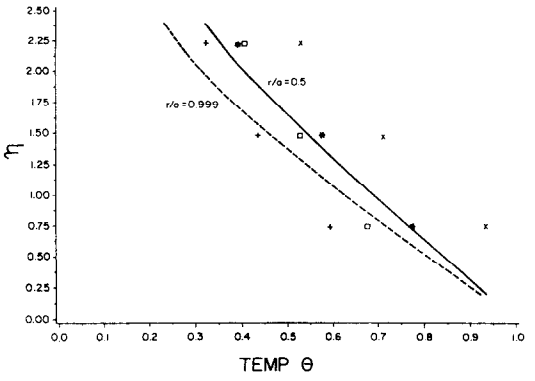

FIG. 9. Comparison of the reconstructed temperatures with numerical predictions at $r/a = 0.79$ and $Gr_a = 1.1 \times 10^5$ at four circumferential locations, +, ×, *, each 90° apart.

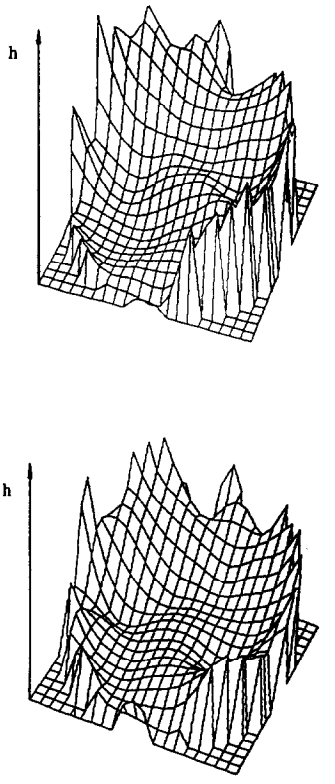

FIG. 10. Local heat transfer coefficients over the disk surface for surface temperatures of 120 and 191°C.

are not valid very near the center of the disk. The results are presented in terms of the non-dimensional variable η defined in the Nomenclature. For a given radial position and disk surface temperature, η increases with elevation. The numerical results are presented near the disk edge, $r/a = 0.99$ and 0.5. The experimental data are presented for $r/a = 0.79$ at four circumferential locations and three elevations. Note that the radial locations of the reconstructed temperatures and the numerical results do not exactly coincide. A comparison of results suggests significant circumferential variation in the experimental data which, however, overlap the numerical predictions. Based on these comparisons the three-dimensional reconstructions of the temperature field are encouraging.

The local heat transfer coefficient distributions obtained for the two surface temperatures are shown in Fig. 10. Consistent with the numerical predictions of ref. [8] the heat transfer coefficient is large near the leading edge and is nearly constant towards the disk center. There are slight minima away from the disk center, this was observed for a different geometry by Al-Arabi and El-Riedy [9] who attributed this to local flow separation.

The spatial average of the local heat transfer coefficients was used to obtain the mean Nusselt number. The characteristic length is the ratio of the disk area to its perimeter. The values are shown in Fig. 11 along with correlations found by Fishenden and Saunders [23], Goldstein *et al.* [24], Lloyd and Moran [25], and Goldstein and Lau [7]. Also included are the results obtained with the same apparatus using a global energy balance technique from ref. [10]. Despite the fact that the reconstructed results are for one instant in time, the spatially averaged heat transfer coefficients for the two surface temperatures studied are in good agreement with other methods.

CONCLUSIONS

Several observations should be made concerning the nature of this problem and the application of holographic interferometry. It has been seen that the natural convection above a horizontal surface is dynamic, with a complex thermal structure that varies with surface temperature. It appears as though there

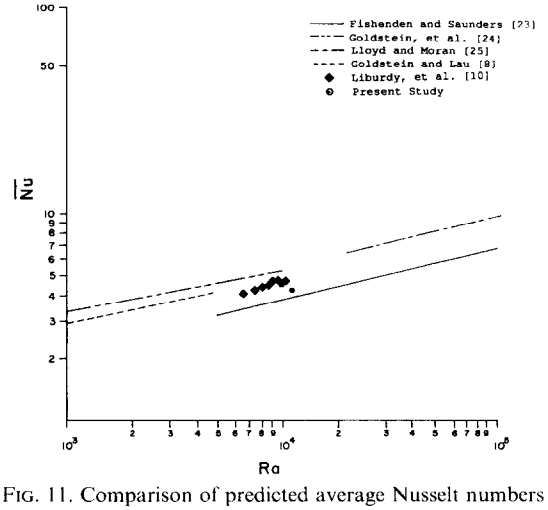

FIG. 11. Comparison of predicted average Nusselt numbers with correlations in the literature.

is significant temporal variation of the local heat transfer coefficient. In order to resolve the nature of the dynamics it will be necessary to obtain three-dimensional time-dependent interferograms. We have shown, in this paper, that the temperature field can be resolved such that the local heat transfer coefficient can be determined. The next step is to obtain sufficient time-dependent information and develop a rapid procedure to digitize, and analyze the interferometric information. The goal is a technique which can interpret three-dimensional transient variations of the local heat transfer conditions. This will aid in the understanding of convective heat transfer and provide a tool to understand instabilities and complex augmentation of heat transfer.

Acknowledgement—The work presented in this paper was funded by the National Science Foundation, Grant CBT-8415360 and is greatly appreciated.

REFERENCES

1. R. B. Husar and E. M. Sparrow, Patterns of free convection flow adjacent to horizontal heated surfaces, *Int. J. Heat Mass Transfer* **11,** 1206–1208 (1968).
2. Z. Rotem and L. Claassen, Natural convection above unconfined horizontal surfaces, *J. Fluid Mech.* **39**(1), 173–192 (1969).
3. L. Pera and B. Gebhart, Natural convection boundary layer flow over horizontal and slightly inclined surfaces, *Int. J. Heat Mass Transfer* **16,** 1131–1146 (1973).
4. K. Stewartson, On the free convection from horizontal plate, *ZAMP* **9a,** 276–282 (1968).
5. J. A. D. Ackroyd, Laminar natural convection on near-horizontal plates, *Proc. R. Soc. Lond.* **A352,** 249–274 (1976).
6. S. B. Robinson and J. A. Liburdy, Prediction of the natural convective heat transfer from a horizontal heated disk, *J. Heat Transfer* **109,** 906–911 (1987).
7. R. J. Goldstein and K. Lau, Laminar natural convection from a horizontal plate and the influence of plate-edge extensions, *J. Fluid Mech.* **129,** 55–75 (1983).
8. B. J. Tsai and J. A. Liburdy, Numerical prediction of natural convection from a horizontal disk, *Proc. 8th Int. Heat Transfer Conf.*, Vol. 2, pp. 441–446 (1986).
9. M. Al-Arabi and M. K. El-Riedy, Natural convection heat transfer from isothermal horizontal plates of different shapes, *Int. J. Heat Mass Transfer* **19,** 1399–1404 (1976).
10. J. A. Liburdy, R. Dorroh and S. Bahl, Experimental investigation of natural convection from a horizontal disk, *Proc. 2nd ASME–JSME Thermal Engng Joint Conf.*, Vol. 3, pp. 605–613 (1987).
11. W. W. Yousef, J. D. Tarasuk and W. J. Mckeen, Free convection heat transfer from upward-facing isothermal horizontal surfaces, *J. Heat Transfer* **104,** 493–500 (1982).
12. S. Bahl and J. A. Liburdy, Three-dimensional image reconstruction from a limited field of view, *IEEE Comput. Soc. 20th SSST Conf. Proc.*, March, Charlotte, North Carolina (1988).
13. D. W. Sweeney and C. M. Vest, Measurement of three dimensional temperature fields above heated surfaces by holographic interferometry, *Int. J. Heat Mass Transfer* **17,** 1443–1453 (1974).
14. C. M. Vest and P. T. Radulovic, Measurement of three-dimensional temperature fields by holographic interferometry. In *Applications of Holography and Data Processing*, pp. 241–249. Pergamon Press, London (1977).
15. C. M. Vest, *Holographic Interferometry*. Wiley, New York (1979).
16. S. Bahl, Studies of three-dimensional natural convection above horizontal heated disks using laser holographic interferometry, Ph.D. Dissertation, Clemson University, Clemson, South Carolina (1988).
17. A. M. Cormack, Representation of a function by its line integral, with some radiological applications, *J. Appl. Phys.* **34,** 2722–2727 (1963).
18. R. N. Bracewell and S. J. Wernecke, Image reconstruction over a finite field of view, *J. Opt. Soc. Am.* **65,** 1342–1346 (1975).
19. S. Cha, Interferometric tomography for three-dimensional flow fields via envelop function and orthogonal series expansions, *Opt. Engng* **27**(7), 557–563 (1988).
20. B. E. Oppenheim, More accurate algorithms for interactive 3-dimensional reconstruction, *IEEE Trans. Nucl. Sci.* **NS-21,** 72–77 (1974).
21. R. Gordon, A tutorial on ART, *IEEE Trans. Nucl. Sci.* **NS-21**(3), 78–93 (1974).
22. P. T. Radulovic, Holographic interferometry of asymmetric temperature or density fields, Ph.D. Dissertation, The University of Michigan, Ann Arbor, Michigan (1977).
23. M. Fishenden and O. A. Saunders, *An Introduction to Heat Transfer*, pp. 96–97. Oxford University Press, London (1950).
24. R. J. Goldstein, E. M. Sparrow and D. C. Jones, Natural convection mass transfer adjacent to horizontal plates, *Int. J. Heat Mass Transfer* **16,** 1025–1035 (1973).
25. J. R. Lloyd and W. R. Moran, Natural convection adjacent to horizontal surfaces of various planforms, *J. Heat Transfer* **96,** 443–447 (1974).

MESURE DU COEFFICIENT DE TRANSFERT LOCAL PAR CONVECTION THERMIQUE PAR INTERFEROMETRIE TRIDIMENSIONNELLE

Résumé—La restitution de la distribution tridimensionnelle de la température au dessus d'un disque horizontal chauffé dans l'air est utilisée pour déterminer les coefficients locaux de transfert thermique. L'interférométrie holographique est utilisée pour obtenir une information instantanée et tridimensionnelle sur la distribution locale de l'indice de réfraction. Plusieurs procédures de traitement sont testées sous la contrainte d'un champ de vision limité et de données d'ordre de frange limitées. Ces techniques sont utilisées pour mesurer avec précision la distribution instantanée et locale de température. Les gradients de température à la surface sont spécifiés par une procédure de calage de courbe et on détermine les coefficients locaux de transfert thermique. Le nombre de Nusselt moyen à la paroi s'accorde bien avec des études antérieures. L'interférométrie holographique en temps réel est aussi utilisée pour suggérer quelques caractéristiques dynamiques du mécanisme de transfert convectif. Les résultats montrent des instabilités locales sous la forme de bouffées distribuées d'énergie thermique à partir de la surface. A des températures élevées le champ entier de température montre à l'évidence une oscillation ou une pulsation qui indique un mécanisme global de libération de chaleur.

MESSUNG ÖRTLICHER WÄRMEÜBERGANGSKOEFFIZIENTEN BEI KONVEKTION MIT HILFE DER DREIDIMENSIONALEN INTERFEROMETRIE

Zusammenfassung—Die dreidimensionale Temperaturverteilung über einer waagerechten beheizten Scheibe, die an Luft grenzt, wird rekonstruiert, um örtliche Wärmeübergangskoeffizienten zu bestimmen. Mit Hilfe der holografischen Interferometrie ergeben sich Informationen über die momentane dreidimensionale Verteilung der örtlichen Brechzahl. Bei den gegebenen Beschränkungen aufgrund des begrenzten Sichtfeldes und der begrenzten Daten über die Ordnung der Interferenzstreifen werden verschiedene Verfahren zur Rekonstruktion erprobt. Diese Verfahren werden für die genaue Messung der Momentan-Temperaturverteilung verwendet. Anschließend werden durch Kurvenanpassung die Temperaturgradienten an der Oberfläche und damit die örtlichen Wärmeübergangskoeffizienten bestimmt. Die oberflächengemittelte Nusselt-Zahl stimmt sehr gut mit früheren Untersuchungen aus der Literatur überein. Die holografische Interferometrie in Echtzeit wird zusätzlich dazu verwendet, einige dynamische Eigenschaften des konvektiven Wärmeübergangs zu ermitteln. Die Ergebnisse zeigen örtliche Instabilitäten, die sich darin äußern, daß an bestimmten Stellen thermische Energie von der Oberfläche "abgesprengt" wird. Bei ausreichend hohen Oberflächentemperaturen ergeben sich aus dem gesamten Temperaturfeld Hinweise auf Oszillationen oder Pulsationen, was auf eine globalen Mechanismus für die Wärmeabgabe hindeutet.

ИЗМЕРЕНИЕ ЛОКАЛЬНЫХ КОЭФФИЦИЕНТОВ КОНВЕКТИВНОГО ТЕПЛОПЕРЕНОСА С ИСПОЛЬЗОВАНИЕМ ТРЕХМЕРНОЙ ИНТЕРФЕРОМЕТРИИ

Аннотация—Для определения локальных коэффициентов теплопереноса используется восстановление трехмерного распределения температур над горизонтальным нагретым диском, помещенным в воздух. Голографическая интерферометрия применяется для получения мгновенной трехмерной информации о распределении локального показателя преломления. Проводится опробование нескольких методов восстановления в условиях ограниченного поля зрения и ограниченных данных о порядке полос. Указанные методы применяются для точного измерения мгновенного локального распределения температур. Затем поверхностные температурные градиенты уточняются подбором эмпирической кривой и определяются локальные коэффициенты теплопереноса. Осредненные по поверхности числа Нуссельта очень хорошо согласуются с результатами ранее опубликованных в литературе исследований. На основе голографической интерферометрии в реальном времени делаются предположения о некоторых динамических характеристиках процесса конвективного теплопереноса. Полученные результаты свидетельствуют о локальной неустойчивости в виде распределенного пика тепловой энергии от поверхности. При достаточно высоких температурах поверхности во всем температурном поле наблюдается осцилляция или пульсация, что указывает на глобальный механизм тепловыделения.